High-Performance Nanocomposites Derived From Allyl-Terminated Benzoxazine and Octakis(propylglycidyl ether) Polyhedral Oligomeric Silsesquioxane

Kai-Wei Huang, Shiao-Wei Kuo
Department of Materials and Optoelectronic Science, Center for Nanoscience and Nanotechnology, National Sun Yat-Sen University, Kaohsiung 804, Taiwan

In this study, we used the Mannich condensation of bisphenol A, formaldehyde, and allylamine to synthesize a allyl-terminated benzoxazine (VB-a), which can be polymerized through ring opening polymerization. We used this VB-a monomer, blended with octakis(propylglycidyl ether) polyhedral oligomeric silsesquioxane (OG-POSS), to prepare polybenzoxazine/POSS nanocomposites. Differential scanning calorimetry and Fourier transform infrared (FTIR) spectroscopy revealed that the mechanism of the crosslinking reaction leading to the formation of the organic/inorganic network involved two steps: (i) ring opening and allyl polymerizations of VB-a and (ii) subsequent reactions between the in situ-formed phenolic hydroxyl groups of VB-a and the epoxide groups of OG-POSS. Dynamic mechanical analysis revealed that the nanocomposites had higher mechanical properties than did the control VB-a. In the glassy state, nanocomposites containing less than 10 wt % POSS displayed enhanced storage moduli; those of the nanocomposites containing greater than 10 wt % POSS were relatively low, due to aggregation, as determined using scanning electron microscopy. Thermogravimetric analysis indicated that the nanocomposites possessed greater thermal stability than that of the pure polymer. FTIR spectroscopic analysis revealed the presence of hydrogen bonding between the siloxane groups of POSS and the OH groups of the polybenzoxazine. POLYM. COMPOS., 32:1086–1094, 2011. © 2011 Society of Plastics Engineers

INTRODUCTION

Much progress has been made recently in developing multicomponent reactive epoxy or polybenzoxazine systems to achieve heterogeneous structures with tailor-made properties [1, 2]. Epoxy resins have excellent chemical resistance to solvents and adhere well to many substrates. Benzoxazines are an intriguing class of cyclic compounds that have attracted considerable attention as cyclic monomers so far. Benzoxazine monomers, heterocyclic compounds featuring an oxazine ring, are synthesized through the reactions of primary amines, phenols, and formaldehyde; they can be polymerized through ring opening polymerization in the absence of a catalyst, releasing no byproduct [3–5]. In addition, polybenzoxazines are polymeric materials of low-surface free energy, because of strong intramolecular hydrogen bonding [6]; therefore, they have wide applicability in superhydrophobic surfaces [7–9], for lithographic patterning [10], and in mold-release materials in nanoimprint technology [11].

The effects of the epoxy concentration on the properties of benzoxazine-epoxy copolymers have been studied extensively from a practical perspective [12]. Copolymerization leads to significant increases in glass transition temperature (T_g), flexural stress, and strain at break, relative to those of polybenzoxazine homopolymers. To further improve the thermal stability of polybenzoxazines, polymerizable allyl and acetyl side groups have been introduced into the benzoxazine monomer [13–20]. Polybenzoxazines prepared from benzoxazines featuring an allyl group (e.g., VB-a) exhibit higher values of T_g ($\sim$300°C), better maintain their storage moduli at higher temperatures, and have superior thermal stabilities than do those of corresponding polybenzoxazines formed from monomers lacking allyl groups. In a previous study, we designed a copolymer network from three reactive groups: an epoxy ring, a benzoxazine ring, and an allyl unit. The phenolic groups formed upon ring opening polymerization of benzoxazine can react with epoxy resins at elevated temperature; meanwhile, homogeneous networks and additional crosslinking points are expected [21]. Notably, this system does not require any added catalyst for epoxy curing, because the phenolic groups of polybenzoxazines can act as initiators and catalysts. Hence, copolymerization of epoxy resin with the allyl benzoxazine monomer VB-a may allow the fabrication of network structures and, thereby, high-performance materials.

Correspondence to: Shiao-Wei Kuo; e-mail: kuosw@faculty.nsysu.edu.tw
Contract grant sponsor: National Science Council, Taiwan, Republic of China; contract grant numbers: NSC 97-2221-E-110-013-MY3, NSC 97-2120-M-009-003.
DOI 10.1002/pc.21126
Published online in Wiley Online Library (wileyonlinelibrary.com).

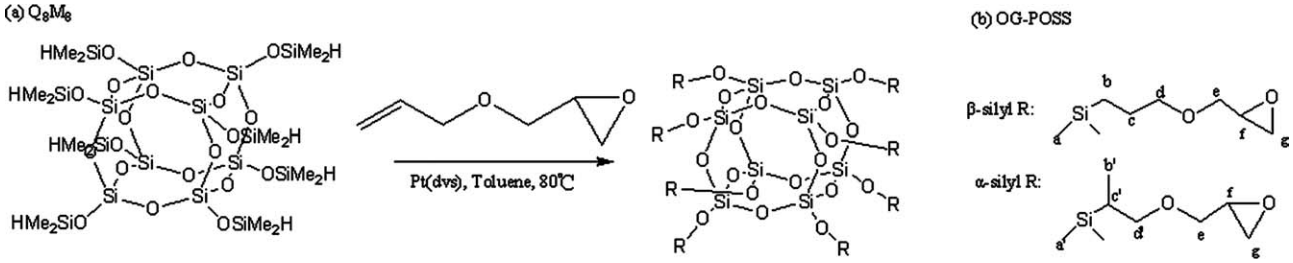

Scheme 1. Chemical structures and reaction sequence for the preparation of (a) $Q_8M_8{}^H$ and (b) OG-POSS.

The incorporation of inorganic silica and silicates (e.g., clay) [22–25] or polyhedral oligomeric silsesquioxane (POSS) reagents [26–34] into the matrix can further improve the performance of polybenzoxazines. Relative to clay or conventional fillers, POSS has the advantages of a monodisperse molecular weight, well-defined structure, low density, high temperature stability, the absence of trace metals, and sizable interfacial interaction between the composite particles and the polymer segments. Highly functionalized POSS monomers can be used to prepare POSS-containing polymer nanocomposites [35–41]. Because POSS compounds may contain one or more reactive sites, they are readily incorporated into common polymers. To improve the properties of the composite material, POSS units presenting polymerizable groups can be introduced into the matrix.

In this study, we combined the advantageous properties of both allyl group-containing benzoxazine and POSS monomers into the polybenzoxazine matrix to enhance the thermal and mechanical properties of the resulting nanocomposites. We synthesized a multifunctional POSS bearing eight epoxy groups (OG-POSS); we then copolymerized it with VB-a benzoxazine monomers through ring opening polymerization. Because these polybenzoxazine/POSS hybrid materials feature large numbers of POSS units in their polybenzoxazines, they exhibit notably improved thermal and mechanical stability, as evidenced through thermogravimetric analysis (TGA) and dynamic mechanical analysis (DMA).

EXPERIMENTAL

Materials

Octakis(dimethylsiloxy)silsesquioxane ($Q_8M_8{}^H$) containing eight hydrosilane groups was purchased from Hybrid Plastics (USA). Allyl glycidyl ether (AGE) and the platinum complex Pt-dvs (2 wt % Pt in xylene) were purchased from Aldrich (USA). Before use, the solution of the Pt complex was diluted 100-fold with xylene. Toluene was dried through distillation. Paraformaldehyde and allylamine were purchased from Tokyo Kasei Kogyo (Japan). The benzoxazine monomer VB-a was prepared according to a literature procedure [28]. The diglycidyl ether of bisphenol A (DGEBA, DER 331; epoxy equivalent weight = 190 g/eq.) was purchased from Dow Chemical (USA).

Multifunctional Octakis(propylglycidyl ether)-POSS

OG-POSS was synthesized through hydrosilylation of AGE with $Q_8M_8{}^H$ (Scheme 1) [42]. The POSS derivative $(HMe_2SiOSiO_{1.5})_8$ (0.50 g, 0.49 mmol) and toluene (5 mL) were stirred magnetically in a 25-mL Schlenk flask. AGE (0.46 mL, 3.92 mmol) was added, followed by 2.0 mM Pt(dvs) (10 drops). The reaction mixture was stirred for 8 h at 80°C; after cooling, dry activated charcoal was added. After stirring for 10 min, the mixture was filtered through a 0.45-μm Teflon membrane. Evaporation of the solvent yielded an opaque viscous liquid (0.86 g, 90%).

Fourier transform infrared (FTIR; cm^{-1}, KBr window): 2900–2850 (—CH_2), 1255 (C—O—C of epoxide), 1090–1000 (Si—O—Si), and 906 (epoxide). ^{1}H Nuclear magnetic resonance (NMR; chloroform-*d*, ppm): 3.72–3.42 [m, $CH_2O(CH_2)_3Si$)] 3.50–3.35 (m, $SiCH_2CH_2CH_2O$; all the resonance between 3.72 and 3.35 were integrated to be 4.0H, 3.16 (OCH_2CH, epoxide, 1.0H), 2.79, 2.60 (CH_2 epoxide, 2.0H), 1.64 ($SiCH_2CH_2CH_2O$, 2.0H), 0.62 ($SiCH_2CH_2CH_2O$, 2.0H). ^{29}Si-NMR ($CDCl_3$, ppm): −1.4 [$(CH_3)_2SiH$] and −107.1 [$SiOSi(CH_3)_2H$]; the latter, three peaks at 10.28 [$(CH_3)_2Si(CHCH_3)$], 12.16 [$(CH_3)_2SiCH_2CH_2$], and −109.23 [$SiOSi(CH_3)_2H$].

OG-POSS Containing VB-a Type Polybenzoxazine Nanocomposites

A mixture of a desired amount of VB-a-type benzoxazine monomer and octakis(propylglycidyl ether) polyhedral oligomeric silsesquioxane (OG-POSS) was stirred for 2 h at room temperature, deposited on an Al plate to dry in the open air for 6 h, and then placed in an oven at 80°C under vacuum for 5 h. The cast film was polymerized in a stepwise manner, at 110°C for 3 h, 160 and 180°C for 2 h each, and then at 200°C for 2 h. The product was postcured at 220°C for 1 h and 240°C for 30 min. Each cured sample was transparent and had a dark red color (film thickness: ~0.2 mm).

Characterizations

^{1}H-NMR spectra were obtained using an INOVA 500 instrument. The samples were dissolved with deuterated

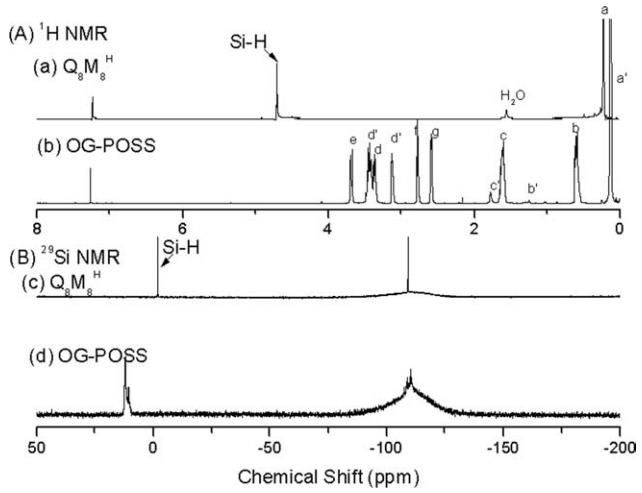

FIG. 1. A: ^{1}H-NMR spectra of (a) $Q_8M_8^H$ and (b) OG-POSS; (B) ^{29}Si-NMR of (c) $Q_8M_8^H$, and (d) OG-POSS in $CDCl_3$.

chloroform ($CDCl_3$), and the solutions were measured with tetramethylsilane as the internal reference. FTIR spectra of the polymer blend films were recorded using the conventional KBr disk method. The films used in this study were sufficiently thin to obey the Beer–Lambert law. FTIR spectra were recorded using a Bruker Tensor 27 FTIR spectrophotometer; 32 scans were collected at a spectral resolution 1 cm^{-1}. Because polymers containing OH groups are hygroscopic, pure N_2 gas was used to purge the spectrometer's optical box to maintain dry sample films. The dynamic curing kinetics was studied using a TA Q-20 differential scanning calorimeter operated under a N_2 atmosphere. The sample (~7 mg) was placed in a sealed Al sample pan. Dynamic curing scans were conducted from 30 to 330°C at a heating rate of 10°C/min. The dynamic mechanical behavior of the cured samples was studied using a DuPont 2980 dynamic mechanical analyzer. The cured sample was polished to ~1.5 × 5.0 × 20.0 mm and mounted on a single cantilever clamp. Constant strain amplitude of 2.0% and a fixed frequency of 1 Hz were used for all measurements. The mechanical properties were measured under N_2 in step mode every 5°C/min from 25 to 350°C. The thermal stability of the samples was characterized using a TA Q-50 thermogravimetric analyzer operated under N_2 atmosphere. The cured sample (~7 mg) was placed in a Pt cell and heated at a rate of 20°C/min from 30 to 800°C at a N_2 flow rate of 60 mL/min. The thermal degradation temperature was taken as the onset temperature at which 20 wt % of weight loss occurs. To observe the phase structures of the polybenzoxazine/POSS nanocomposites, samples were prepared through a curing reaction. The surfaces were coated with thin layers of Au (~100 Å). All specimens were examined with a FEI Quanta 200 environmental scanning electron microscope operated at 20 kV. Transmission electron microscopy (TEM) was performed using a Hitachi H-7100 electron microscope operated at 100 kV. Ultrathin sections of the samples were prepared using a Leica Ultracut S microtome equipped with a diamond knife. Slices of ca. 700 Å thickness were cut at room temperature. The ultrathin sections were placed onto Cu grids coated with carbon-supporting films without staining.

RESULTS AND DISCUSSION

Synthesis of OG-POSS

Hydrosilylation of AGE with $Q_8M_8^H$, mediated by the Karstedt catalyst, provided the octafunctional silsesquioxane octakis(propylglycidyl ether) polyhedral oligomeric silsesquioxane (OG-POSS). Figure 1A-a displays the ^{1}H-NMR spectrum of $Q_8M_8^H$. The spectrum in OG-POSS (Fig. 1A-b) reveals that the allyl groups of the glycidyl ether underwent hydrosilylation to form products having both α and β configurations; signals for the allyl (~5.8 ppm) and Si—H protons (4.7 ppm) were absent, suggesting a quite high conversation of Si—H units under the reaction conditions [42]. In the ^{29}Si-NMR spectra of $Q_8M_8^H$ and OG-POSS (Fig. 1B), the former features two peaks at −1.4 and −107.1 ppm [33]; the latter, three peaks at 10.28, 12.16, and −109.23 ppm. The downfield shifts from −1.4 to 10.28 and 12.16 ppm confirm that the hydrosilylation occurred to completion under the reaction conditions. The signal of methyl group protons was too weak to detect in the ^{1}H-NMR spectrum of OG-POSS, implying that the portion of α addition products was very small and, therefore, that β addition dominated in the hydrosilylation under these conditions.

Figure 2 presents the FTIR spectra of $Q_8M_8^H$ and OG-POSS. The strong absorption peak at ca. 1100 cm^{-1} represents the vibrations of the siloxane Si—O—Si groups and is a general feature of POSS derivatives. The characteristic stretching vibration of the Si—H groups appears as a signal at 2200 cm^{-1} (Fig. 2a). In the FTIR spectrum of OG-POSS, we attribute the band at 906 cm^{-1} to the

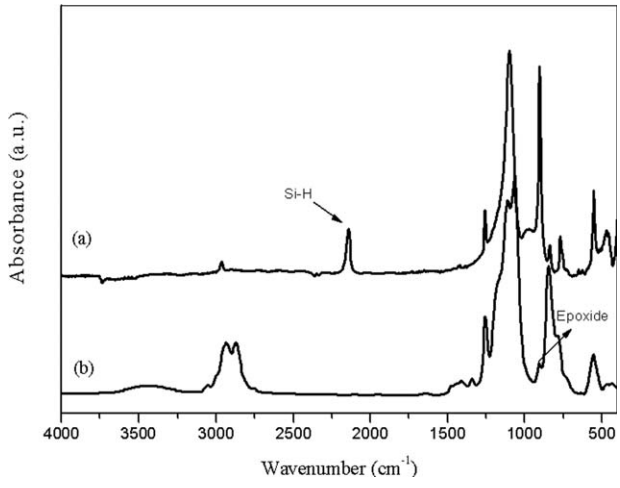

FIG. 2. FTIR spectra of (a) $Q_8M_8^H$ and (b) OG-POSS.

DOI 10.1002/pc

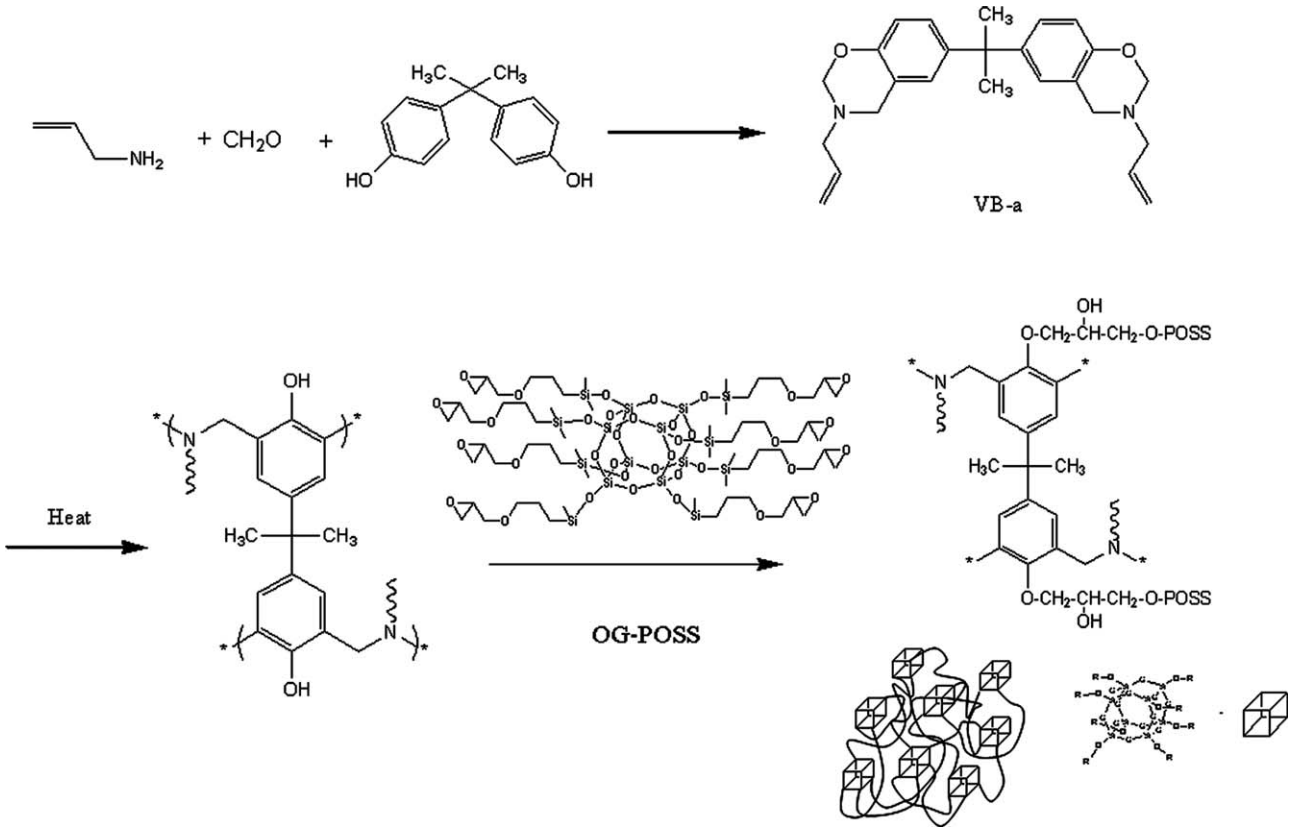

Scheme 2. Possible morphology of the VB-a/OG-POSS blends after thermal curing.

stretching vibrations of the epoxide groups. The absence of a stretching vibration band at 2200 cm^{-1} indicates that the hydrosilylation had occurred to completion. Thus, the ^{1}H-NMR and FTIR spectra are consistent with the formation of OG-POSS.

Curing Behavior of VB-a/OG-POSS Nanocomposites

Polybenzoxazine/POSS nanocomposite materials possess many desirable mechanical properties, including low moisture absorption, high solvent resistance, and improved thermal stability, and certain desirable electronic properties. Scheme 2 outlines our preparation of the polybenzoxazine/POSS composites. Both the VB-a monomer and octakis(propylglycidyl ether) polyhedral oligomeric silsesquioxane (OG-POSS) are soluble in THF and acetone. To synthesize hybrid polymers containing different POSS contents, these readily processable monomers can transformed through (1) ring opening polymerization of VB-a at elevated temperature and (2) subsequent reactions between the phenolic OH groups of PVB-a and the epoxide groups of OG-POSS. The first reaction afford a great number of phenolic OH groups in the macromolecular backbone of PVB-a (Scheme 2); the second reaction creates additional crosslinks between the PVB-a networks and OG-POSS. Prior to curing, the mixtures of VB-a and OG-POSS were all homogeneous and transparent, suggesting that the two components were completely miscible in the composition range investigated.

Figure 3 displays the curing exotherms of neat VB-a, neat OG-POSS, and their binary mixtures at various compositions. Two exotherms appeared for pure VB-a at a heating rate of 10°C/min: the onset temperature of the first exotherm was ca. 170°C, with an exotherm peak at 210°C; the apparent onset of the second exotherm was at 250°C, with an exotherm maximum at 267°C [32]. We

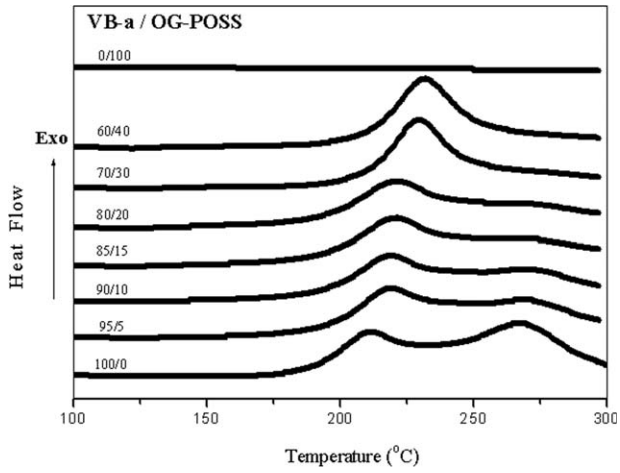

FIG. 3. Curing behavior, determined through DSC analyses, of VB-a/OG-POSS mixtures containing various OG-POSS contents.

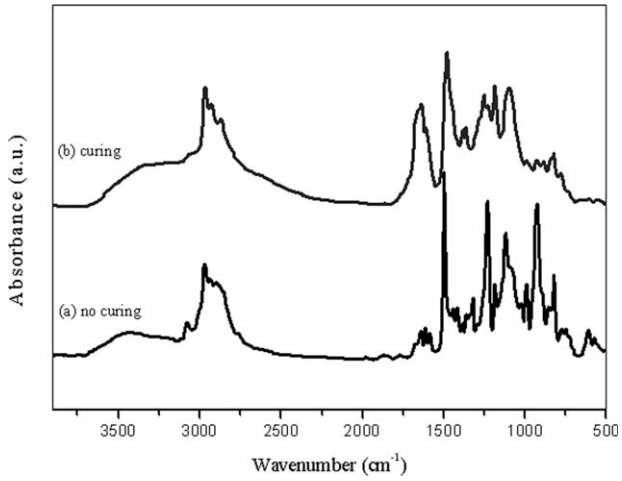

FIG. 4. FTIR spectra of the VB-a/OG-POSS = 90/10 blend (a) before curing and (b) after treatment at 200°C.

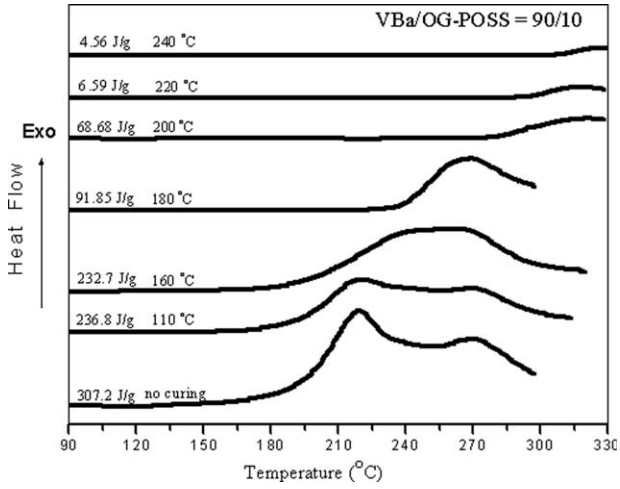

FIG. 5. DSC curve of the VB-a/OG-POSS = 90/10 blend after each stage of curing.

ascribe the first exotherm to thermal curing of the allyl groups; the second exotherm, to ring opening of the oxazine ring, as discussed previously [14]. Upon increasing the OG-POSS concentration, two exotherms merged to become a single peak. The first peak shifted to higher temperature, between 210 and 232°C, presumably because the dilution effect of OG-POSS decreased the curing behavior of the VB-a monomer. The higher temperature (266°C) of the ring opening polymerization of pure VB-a was due to the restricted mobility of the VB-a monomer units after the polymerization of the allyl groups [14]. Notably, pure OG-POSS did not provide an exotherm curve because of the absence of a crosslinking agent for its epoxide groups.

Figure 4 presents FTIR spectra of the uncured and cured VB-a/OG-POSS = 90/10 mixture. The significant decreases in intensity of the bands at 948 and 1232 cm^{-1}, which represent benzoxazine rings, imply that ring opening reactions had occurred, as confirmed by the appearance of a new distribution of bands within the range 2500–3600 cm^{-1}, which we assign to the hydrogen-bonded OH units of the opened oxazine ring species. In addition, a new band for the tetrasubstituted aromatic rings of the polymerized VB-a appears at 1480 cm^{-1}, with a corresponding decrease in intensity of the band at 1498 cm^{-1} representing the trisubstituted aromatic rings of VB-a. Notably, the signal at 915 cm^{-1} for the epoxide units also almost completely vanished for all of the POSS-containing hybrid composites, indicating that OG-POSS participated in the crosslinking reaction. In addition, the characteristic absorption bands of the allyl group at 3080 and 991 cm^{-1} disappeared, confirming the occurrence of the curing reaction.

Figure 5 displays DSC curves of VB-a/OG-POSS = 90/10 after curing at various temperatures. Two exotherms were observed, similar to that of pure VB-a, at a heating rate of 10°C/min. The onset temperature of the first exotherm was ca. 170°C, with the exotherm peak at 220°C; the apparent onset of the second exotherm was at 250°C, with the exotherm maximum at 270°C [14]. The total amount of thermal energy released by VB-a/OG-POSS = 90/10 was 307.2 J/g. The amount of energy released during the second exotherm decreased upon increasing the curing temperature, almost disappearing after curing at 240°C [14].

To confirm which reaction was occurring during each exotherm in the DSC trace, we used FTIR spectroscopy to characterize the curing products from VB-a/OG-POSS = 90/10 at different temperatures (see Fig. 6). The characteristic absorption bands of the allyl group at 3080 and 991 cm^{-1} disappeared after curing at 180°C. Figure 6a reveals that a new band for the tetrasubstituted aromatic rings of the polymerized VB-a appeared at 1480 cm^{-1}, with a corresponding decreases in intensity of the bands representing the trisubstituted aromatic rings of VB-a

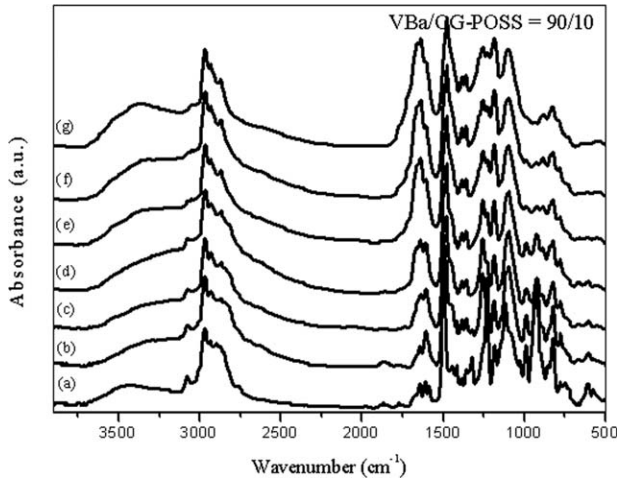

FIG. 6. FTIR spectra of the VB-a/OG-POSS = 90/10 blend (a) before curing and (b-g) after curing at (b) 110, (c)160, (d) 180, (e) 200, (f) 220, and (g) 240°C.

DOI 10.1002/pc

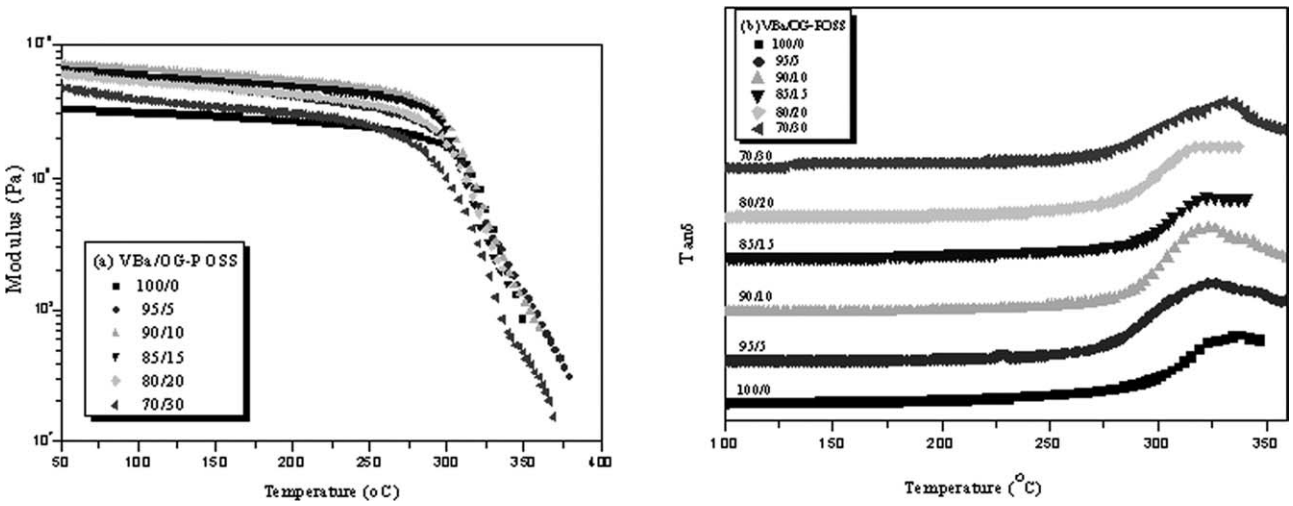

FIG. 7. DMA analyses—(a) storage modulus and (b) tan δ—of VB-a/OG-POSS blends containing various OG-POSS contents, after curing.

(1498 and 943 cm^{-1}), assigned to the trisubstituted benzene ring in the benzoxazine structure. We assign the broad absorptions at 2500–3500 cm^{-1} in Fig. 6b–g to three different kinds of hydrogen bonding interactions; the presence of OH···O intermolecular hydrogen bonding manifests itself in the signal at ca. 3420 cm^{-1}, as discussed previously [43]. More importantly, the maximum peak position of the signal for the siloxane vibrations shifted from 1117 cm^{-1} for the uncured VB-a/OG-POSS = 90/10 (Fig. 6a) to 1100 cm^{-1} after thermal curing (cf. Fig. 6b–g). These results suggest that the siloxane groups of POSS interacted with the OH groups of the polybenzoxazine [44, 45].

Figure 7 presents storage modulus (E') and loss tan δ curves of the polymerized VB-a and OG-POSS hybrids incorporating various contents of OG-POSS. In Fig. 7a, the initial storage modulus (E') of the plain polymerized VB-a (PVB-a) was 3280 MPa at 50°C. The initial values of E' of the hybrids containing 5, 10, 15, 20, and 30 wt % OG-POSS were 6310, 7170, 6570, 6070, and 4770 MPa, respectively, at 50°C. The values of E' of the hybrids increased drastically upon increasing the POSS content to 10 wt %, but decreased thereafter, presumably because of two opposing effects of the POSS cages on the matrices. One, the nanoreinforcement effect of POSS on the polybenzoxazine matrix, tended to increase the modulus of the material; the other, the inclusion of POSS in the system, decreased the density of the nanocomposites. In these organic/inorganic hybrid materials, the cubic silsesquioxane core is rigid, with eight curable epoxide groups appended to the silsesquioxane cores via SiO linkages. In a network structure, the value of T_g relates directly to the cross-linking density [46]. The loss tan δ peak temperature obtained through DMA represents the glass transition temperature of a material. Figure 7b reveals the value of T_g of the P(VB-a) was 327°C, while those of the hybrids containing 5, 10, 15, 20, and 30 wt % OG-POSS were 323, 326, 324, 326, and 330°C, respectively. Thus, the glass transition temperatures of these VB-a polybenzoxazine/POSS nanocomposites did not

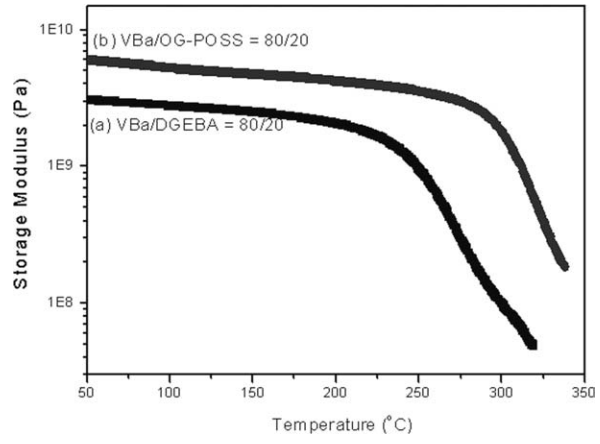

FIG. 8. Storage moduli of the VB-a/OG-POSS = 80/20 and VB-a/DGEBA = 80/20 blends after curing.

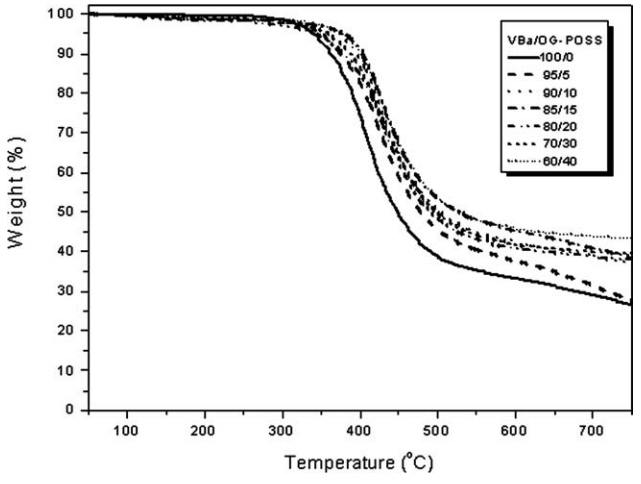

FIG. 9. TGA analyses of VB-a/OG-POSS blends containing various OG-POSS contents, after curing.

TABLE 1. Thermal properties of poly(VB-a)/POSS nanocomposites.

Sample	DMA			TGA	
	G' (MPa)[a]	G'' (°C)	tan δ (°C)	T_{20} (°C)	Char yield (%)[b]
Poly(VB-a)	3304	311	327	390	24.7
5 wt % OG-POSS	6316	315	323	406	23.5
10 wt % OG-POSS	7167	319	326	421	35.6
15 wt % OG-POSS	6565	314	324	425	36.2
20 wt % OG-POSS	6067	317	326	413	37.7
30 wt % OG-POSS	4773	319	330	416	39.1
40 wt % OG-POSS	ND[c]	ND[c]	ND[c]	423	43.1

[a] Measured at 50°C.
[b] Measured at 800°C.
[c] Pure OG-POSS and 40 wt % OG-POSS could not be induced to form films.

change upon increasing the OG-POSS content, due to two opposing and competing effects. The glass transition behavior cannot be explained solely on the basis of the so-called nanoreinforcement effect. In fact, the inclusion of the bulky POSS cages increases the free volume of the polymer matrix; the result should be a depression of T_g, as has been observed for other POSS-containing nanocomposites [46, 47]. From a comparison of the VB-a/OG-POSS and VB-a/DGEBA = 80/20 systems, however, the storage modulus and value of T_g of VB-a/POSS were much higher than those of the VB-a/DGEBA system, indicating that the presence of the bulky and rigid POSS nanoparticles (NPs) tended to stiffen the crosslinked poly-

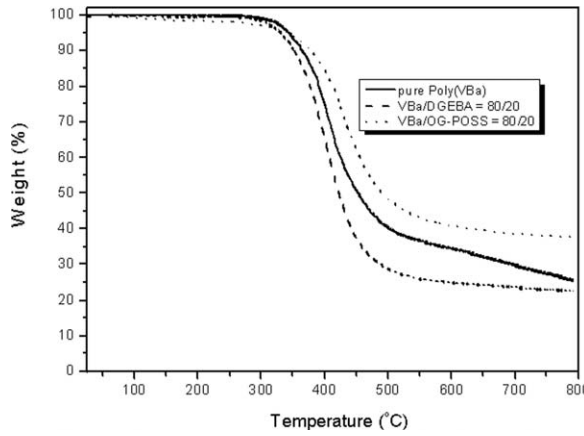

FIG. 10. TGA analyses of pure poly(VB-a) and the VB-a/OG-POSS = 80/20 and VB-a/DGEBA = 80/20 blends, after curing.

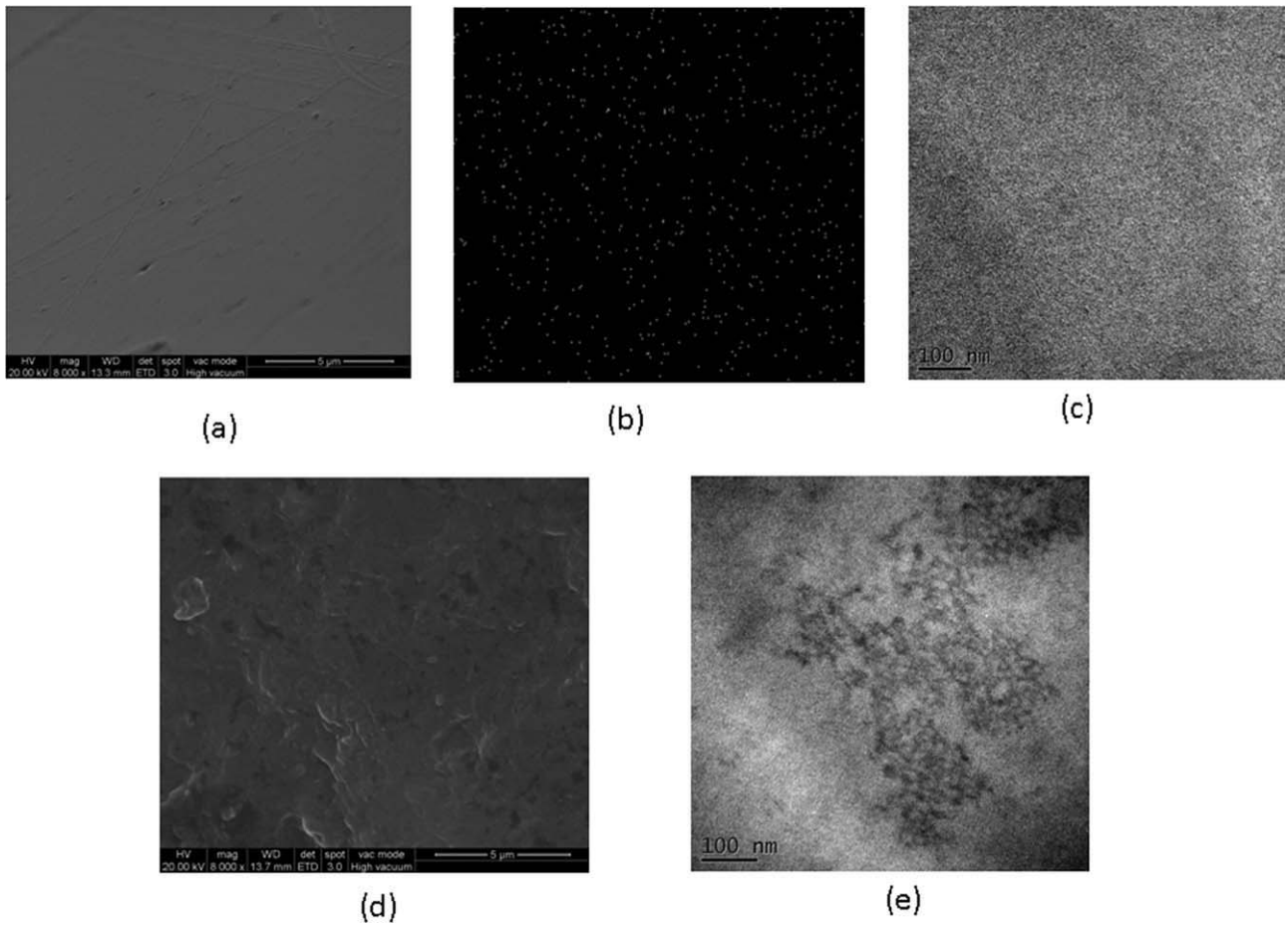

FIG. 11. (a) SEM, (b) Si-mapping from (a), and (c) TEM images of VB-a/OG-POSS = 85/15. (d) SEM and (e) TEM images of VB-a/OG-POSS = 60/40.

 DOI 10.1002/pc

benzoxazine network, resulting in significant increase in its values of E' and T_g as shown in Figure 8.

Figure 9 reveals the thermal stabilities under N_2 of the polybenzoxazine/POSS nanocomposites. Table 1 summarizes the thermal properties of the polybenzoxazine/POSS nanocomposites tested in this study. To compare the thermal stabilities, we used the 20 wt % weight loss temperature as a standard. The decomposition temperature (T_d) of the polybenzoxazine/POSS nanocomposites gradually increased upon increasing the OG-POSS content up to 15%. Further increases in the OG-POSS content caused the decomposition temperature to decrease, due to a similar phenomenon as that for the trend in the storage modulus. The variation in thermal stability, as measured in terms of the decomposition temperature, may be construed as an effect of creating nanocomposites. In a nanocomposite material, thermal motion of the tether units is restricted, thereby reducing the organic decomposition pathways accessible to the tether. The char yield, another indicator of thermal stability, also increased upon increasing the POSS content, relative to VB-a monomer, in these hybrid materials. For these hybrids, increasing the POSS content should improve a composite's thermal properties. Our results indicate that the thermal stability of polybenzoxazines is improved through the formation of network structures with the incorporated inorganic silsesquioxane. From a comparison of VB-a/OG-POSS and VB-a/DGEBA = 80/20 systems (see Fig. 10), the values of T_d and char yield of VB-a/POSS were much higher than those of the VB-a/DGEBA system, indicating that the presence of the bulky and rigid POSS NPs tended to stiffen the cross-linked polybenzoxazine network, resulting in a significant increase in decomposition temperature. During the early stages of combustion of these polymer/POSS nanocomposites, the POSS units might evolve into a ceramic superficial layer because of the low surface energy of the siloxane structure of POSS [48]; this ceramic layer would protect the underlying material by limiting heat transfer and hampering the diffusion of O_2 and the evacuation of combustible products, in analogy with the behavior of layered silicates [22].

Next, we used scanning electron microscopy (SEM) and TEM to examine the homogeneity of the POSS NP dispersion. Figure 11a displays SEM images of the polybenzoxazine/POSS nanocomposite having a POSS content of 15 wt %; we observe a featureless morphology, with no discernible phase separation, suggesting that POSS NPs are homogeneously dispersed throughout the matrix. The EDX Si-mapping of all of the composites revealed that the particles were uniformly dispersed in the cross-sectional surfaces observed (Fig. 11b). The yellow points in the image denote POSS-enriched regions. The Si-mapping micrograph reveals no aggregation; rather, it indicates many spherical particles (4–5 nm in diameter) uniformly dispersed, which is confirmed by TEM image in Fig. 11c. When the concentration of POSS was 40 wt %, the SEM and TEM images revealed aggregation from Fig. 11d and e, respectively. Serious aggregation of OG-POSS occurred in the VB-a-type polybenzoxazine matrix because of lower miscibility at higher OG-POSS contents, consistent with the thermal properties determined through DSC, TGA, and DMA analyses.

CONCLUSIONS

After synthesizing octakis(propylglycidyl ether)-POSS (OG-POSS) through hydrosilylation of AGE with $Q_8M_8^H$, we prepared polybenzoxazine/POSS composites having various OG-POSS contents and used DSC, TGA, and DMA analyses to examine their thermal properties. The storage moduli and decomposition temperatures of these nanocomposites improved after incorporating OG-POSS, a result of hydrogen bonding between the siloxane groups of POSS and the OH groups of the polybenzoxazine, as determined through FTIR spectroscopic analysis. When the OG-POSS content was greater than 20 wt %, however, aggregation of the POSS units resulted in poorer thermal properties.

REFERENCES

1. W.J. Burke, K.C. Murdock, and E. Grace, *Am. Chem. Soc.*, **76**, 1677 (1954).
2. W.J. Burke, C. Weatherbee, H. Lau, G.V. Lear, and G. Goken, *J. Org. Chem.*, **4**, 1099 (1963).
3. T. Takeichi, T. Kawauchi, and T. Agag, *Polym. J.*, **40**, 1121 (2008).
4. C.P.R. Nair, *Prog. Polym. Sci.*, **29**, 401 (2004).
5. N.N. Ghosh, B. Kiskan, and Y. Yagci, *Prog. Polym. Sci.*, **32**, 1344 (2007).
6. C.F. Wang, Y.C. Su, S.W. Kuo, C.F. Huang, Y.C. Sheen, and F.C. Chang, *Angew. Chem. Int. Ed.*, **45**, 2248 (2006).
7. C.F. Wang, S.H. Chiou, F.H. Ko, C.T. Chou, H.C. Lin, C.F. Hunag, and F.C. Chang, *Macromol. Rapid. Commun.*, **27**, 333 (2006).
8. C.F. Wang, Y.T. Wang, P.H. Tung, S.W. Kuo, C.H. Lin, Y.C. Sheen, and F.C. Chang, *Langmuir*, **22**, 8289 (2006).
9. C.S. Liao, C.F. Wang, H.C. Lin, H.Y. Chou, and F.C. Chang, *Langmuir*, **25**, 3359 (2009).
10. C.S. Liao, C.F. Wang, H.C. Lin, H.Y. Chou, and F.C. Chang, *J. Phys. Chem. C*, **112**, 16189 (2008).
11. C.F. Wang, S.F. Chiou, F.H. Ko, J.K. Chen, C.T. Chou, C.F. Huang, S.W. Kuo, and F. C. Chang, *Langmuir*, **23**, 5868 (2007).
12. B.S. Rao, K.R. Reddy, S.K. Pathak, and A.R. Pasala, *Polym. Int.*, **54**, 1371 (2005).
13. A. Chernykh, T. Agag, and H. Ishida, *Polymer*, **50**, 3153 (2009).
14. T. Agag, and T. Takeichi, *Macromolecules*, **34**, 7257 (2001).
15. T. Agag, and T. Takeichi, *Macromolecules*, **36**, 6010 (2003).
16. T. Takeichi, K. Nakamura, T. Agag, and H. Muto, *Des. Mono. Polym.*, **7**, 727 (2004).

17. K.S. Kumar, C.P. Nair, T.S. Radhakrishnan, and K.N. Ninan, *Eur. Polym. J.*, **43**, 2504 (2007).
18. B. Kiskan and Y. Yagci, *Polymer*, **49**, 2455 (2004).
19. B. Kiskan, B. Aydoan, and Y. Yagci, *J. Polym. Sci., Part A: Polym. Chem.*, **47**, 804 (2009).
20. A. Chernykh, T. Agag, and H. Ishida, *Macromolecules*, **42**, 5121 (2009).
21. S.W. Kuo and W.C. Liu, *J. Appl. Polym. Sci.*, **117**, 3121 (2010).
22. H.K. Fu, C.F. Huang, S.W. Kuo, H.C. Lin, D.R. Yei, and F.C. Chang, *Macromol. Rapid. Commun.*, **29**, 1216 (2008).
23. T. Agag and T. Takeichi, *Polym. Comp.*, 750 (2008).
24. Z. Shi, D. Yu, Y. Wang, and R. Xu, *J. Appl. Polym. Sci.*, **88**, 194 (2003).
25. S.A. Garea, H. Iovu, A. Nicolescu, and C. Deleanu, *Polym. Test.*, **28**, 338 (2009).
26. Y.J. Lee, S.W. Kuo, Y.C. Su, J.K. Chen, W.C. Chen, C.W. Tu, and F.C. Chang, *Polymer*, **45**, 6321 (2004).
27. Y.J. Lee, J.M. Huang, S.W. Kuo, J.K. Chen, and F.C. Chang, *Polymer*, **46**, 2320 (2005).
28. Y.J. Lee, S.W. Kuo, C.F. Huang, and F.C. Chang, *Polymer*, **47**, 4378 (2006).
29. Q. Chen, R.W. Xu, J. Zhang, and D.S. Yu, *Macromol. Rapid. Commun.*, **26**, 1878 (2005).
30. J. Zhang, R.W. Xu, and D.S. Yu, *Eur. Polym. J.*, **43**, 743 (2007).
31. Y.H. Liu and S. Zheng, *J. Polym. Sci., Part A: Polym. Chem.*, **44**, 1168 (2006).
32. S.W. Kuo and K.W. Huang, *Macromol. Chem. Phys.*, **211**, 2301 (2010).
33. Y.C. Wu and S.W. Kuo, *Polymer*, **51**, 3948 (2010).
34. J.M. Huang, S.W. Kuo, H.J. Huagn, Y.X. Wang, and Y.T. Chen, *J. Appl. Polym. Sci.*, **111**, 628 (2009).
35. C.H. Lu, J.H. Wang, F.C. Chang, and S.W. Kuo, *Macromol. Chem. Phys.*, **211**, 1339 (2010).
36. C.H. Lu, S.W. Kuo, W.T. Chang, and F.C. Chang, *Macromol. Rapid. Commun.*, **30**, 2121 (2009).
37. K.W. Huang, L.W. Tsai, and S.W. Kuo, *Polymer*, **50**, 4876 (2009).
38. S.W. Kuo, Y.C. Wu, C.H. Lu, and F.C. Chang, *J. Polym. Sci. Part B: Polym. Phys.*, **47**, 811 (2009).
39. S.W. Kuo, H.F. Lee, W.J. Huang, K.U. Jeong, and F.C. Chang, *Macromolecules*, **42**, 1619 (2009).
40. Y.J. Yen, S.W. Kuo, C.F. Huang, J.K. Chen, and F.C. Chang, *J. Phys. Chem. B*, **112**, 10821 (2008).
41. H.Y. Xu, S.W. Kuo, J.S. Lee, and F.C. Chang, *Macromolecules*, **35**, 8788 (2002).
42. W.Y. Chen, Y.Z. Wang, S.W. Kuo, C.F. Huang, P.H. Tung, and F.C. Chang, *Polymer*, **45**, 6897 (2004).
43. H.D. Kim and H. Ishida, *J. Phys. Chem. A*, **106**, 3271 (2002).
44. S.W. Kuo, H.C. Lin, W.J. Huang, C.F. Huang, and F.C. Chang, *J. Polym. Sci., Part B: Polym. Phys.*, **44**, 673 (2006).
45. H.Y. Xu, S.W. Kuo, and F.C. Chang, *Polym. Bull.*, **48**, 469 (2002).
46. C.M. Leu, Y.T. Chang, and K.H. Wei, *Chem. Mater.*, **15**, 3721 (2003).
47. C.M. Leu, G. Reddy, K.H. Wei, and C.F. Shu, *Chem. Mater.*, **15**, 2261 (2004).
48. H.C. Lin, S.W. Kuo, C.F. Huang, and F.C. Chang, *Macromol. Rapid. Commun.*, **27**, 537 (2006).

 DOI 10.1002/pc